Cell Death & Differentiation (2019) 26:470–486
https://doi.org/10.1038/s41418-018-0131-6

Cell Death & Differentiation

ARTICLE

DNase II activated by the mitochondrial apoptotic pathway regulates RIP1-dependent non-apoptotic hepatocyte death via the TLR9/IFN-β signaling pathway

Yoshinobu Saito[1] · Hayato Hikita[1] · Yasutoshi Nozaki[1] · Yugo Kai[1] · Yuki Makino[1] · Tasuku Nakabori[1] · Satoshi Tanaka[1] · Ryoko Yamada[1] · Minoru Shigekawa[1] · Takahiro Kodama[1] · Ryotaro Sakamori[1] · Tomohide Tatsumi[1] · Tetsuo Takehara[1]

Received: 2 October 2017 / Revised: 6 May 2018 / Accepted: 8 May 2018 / Published online: 31 May 2018

Abstract

Cell death, including apoptotic and non-apoptotic cell death, is frequently observed in liver disease. Upon activation of the mitochondrial apoptotic pathway, mitochondria release not only apoptogenic cytochrome *c* but also mitochondrial DNA (mtDNA) into the cytosol. The impact of DNase II, a lysosomal acid DNase that degrades mtDNA, on hepatocyte death remains unclear. Administration of ABT-737, a Bcl-xL inhibitor, upregulated DNase II activity in murine hepatocyte cell line BNL CL.2 cells and induced apoptosis. In cells treated with DNase II siRNA, ABT-737 led to accumulation of mtDNA in the cytosol and increased expression of interferon (IFN)-β and induction of propidium iodide (PI)-positive cells, in addition to apoptosis. Induced PI-positive cells were suppressed by RIP1 inhibitor, Necrostatin-1, but not by pan-caspase inhibitor, ZVAD-FMK, suggesting non-apoptotic cell death. Both the increase in IFN-β and the induction of non-apoptotic cell death were abolished by administering a TLR9 antagonist, ODN2088, or by the removal of mtDNA from cells with ethidium bromide. Hepatocyte-specific Mcl-1 knockout mice developed hepatocyte apoptosis accompanied by upregulated DNase II activity in their livers. Further knockout of DNase II induced IFN-β expression and RIP1-dependent non-apoptotic hepatocyte death, both of which were suppressed by the administration of ODN2088. Mice fed a high-fat diet (HFD), an obesity-associated fatty liver model, showed increased expression of IFN-β with suppression of DNase II activity in their livers and developed not only hepatocyte apoptosis but also non-apoptotic hepatocyte death. Hepatocyte-specific knockout of DNase II exacerbated HFD-induced non-apoptotic hepatocyte death and liver fibrosis. In conclusion, without DNase II, apoptotic stimulation on hepatocytes induces TLR9-dependent IFN-β production and RIP1-dependent non-apoptotic cell death originating from mtDNA. In fatty livers, DNase II activity is suppressed in contrast to simple inactivation of Bcl-xL or Mcl-1, and both apoptotic and non-apoptotic hepatocyte death can develop, leading to the progression of liver fibrosis.

Introduction

Hepatocyte death is observed in various types of liver diseases, such as non-alcoholic fatty liver disease (NAFLD), alcoholic liver disease and viral hepatitis [1]. Mitochondria play a pivotal role in the cell signaling that leads to hepatocyte death, including apoptosis [2, 3], necrosis [4, 5] and necroptosis [6]. Mitochondrial outer membrane permeabilization (MOMP) is a hallmark of the transduction of multiple signals that lead to apoptosis [7, 8]. Bcl-2 homologous antagonist/killer (Bak)/ Bcl-2 associated X protein (Bax) activation leads to MOMP, resulting in the release of not only cytochrome *c* but also mitochondrial DNA (mtDNA) from mitochondria [9, 10]. Released mtDNA regulates the induction of type I interferon (IFN) and the inflammatory response in the absence of active caspase in hematopoietic cells [9, 10]. In cardiomyocytes, undegraded intracellular mtDNA is associated with the pathogenesis of myocarditis and dilated cardiomyopathy [11]. mtDNA is

Edited by H.-U. Simon

Electronic supplementary material The online version of this article (https://doi.org/10.1038/s41418-018-0131-6) contains supplementary material, which is available to authorized users.

✉ Tetsuo Takehara
takehara@gh.med.osaka-u.ac.jp

[1] Department of Gastroenterology and Hepatology, Osaka University Graduate School of Medicine, Osaka, Japan

SPRINGER NATURE
CDDpress

degraded by DNase II, a lysosomal acid DNase, which is encoded by *Dnase2a* [12]. However, the impact of released mtDNA and DNase II activity on hepatocyte death requires clarification.

NAFLD is one of the most common liver diseases worldwide [13] and comprises a wide spectrum of diseases, ranging from simple steatosis to non-alcoholic steatohepatitis (NASH). One of the pathological features of NASH is hepatocyte apoptosis [14, 15]. Necro-inflammation is another important histological characteristic of NASH [16, 17]. Receptor-interacting protein 3 (RIP3), which is a critical mediator of hepatocyte necrosis [6], is elevated in the livers of NASH patients [18, 19]. Disruption of RIP3 attenuates necro-inflammation, liver injury and liver fibrosis in experimental mouse NASH models [18, 19]. Necrotic cells release higher levels of damage-associated molecular patterns (DAMPs) than apoptotic cells and might trigger an inflammatory response [20–22], suggesting the possible importance of hepatocyte non-apoptotic cell death for progression of NASH. However, the mechanism by which hepatocytes undergo non-apoptotic cell death in NASH remains unclear.

Here, we reveal a novel signaling pathway in which receptor-interacting protein 1 (RIP1)-dependent non-apoptotic hepatocyte death is induced via Toll-like receptor 9 (TLR9)/IFN-β signaling accompanied by reduced DNase II activity upon hepatocyte apoptosis induction. The livers of high-fat diet (HFD)-fed mice exhibited suppressed DNase II activity that lead to both apoptotic and non-apoptotic cell death. This report provides the first description of the protective role of DNase II activity in non-apoptotic hepatocyte death with necrotic phenotype upon activation of the mitochondrial apoptosis pathway. Our results demonstrate that the suppression of DNase II activity in NASH livers might affect the progression of NAFLD.

Results

Activation of the mitochondrial apoptotic pathway elevates DNase II activity in CL2 cells and induces PI-positive cells in DNase II-knockdown CL2 cells

Murine hepatocyte cell line BNL CL.2 (CL2) cells were treated with ABT-737, an inhibitor of B-cell lymphoma-extra large (Bcl-xL), which is an essential anti-apoptotic protein in hepatocytes [2]. The percentage of apoptotic cells peaked at 6 h and was accompanied by the activation of caspase-3/7 (Sup.Fig.1A, Sup.Fig.1B). With the appearance of apoptosis, the amount of viable cells decreased (Sup. Fig.1C). Interestingly, DNase II activity in CL2 cells significantly increased 3 h after ABT-737 treatment (Fig. 1a). To investigate the significance of DNase II in hepatocytes, we compared the responses to ABT-737 for cells pretreated with DNase II small interfering RNA (siRNA) to those pretreated with control siRNA. DNase II siRNA transfection reduced its mRNA expression and activity (Sup. Fig.2A, Sup.Fig.2B). Both caspase-3/7 activity and apoptotic cells, which were defined as annexin-V-positive and 7-aminoactinomycin D (7-AAD)-negative cells, in DNase II siRNA-transfected cells did not increase compared with those in control siRNA-transfected cells (Fig. 1b, Sup. Fig.2C). The viability of DNase II siRNA-transfected cells significantly decreased compared with that of the control siRNA-transfected cells (Fig. 1c, Sup.Fig.2D). We found that propidium iodide (PI)-positive cells increased in DNase II siRNA-transfected cells treated with ABT-737 (Fig. 1d, Sup.Fig.2F). The amount of mtDNA isolated from the cytosolic fractions did not differ between the DNase II siRNA-transfected cells and the control siRNA-transfected cells at baseline (Fig. 1e). However, upon ABT-737 treatment, the amount of mtDNA clearly increased and, importantly, was significantly higher in DNase II siRNA-transfected cells than in control siRNA-transfected cells (Fig. 1e). Increase of mtDNA by ABT-737 was also detected in primary hepatocytes isolated from wild-type (WT) mice but not at all in those isolated from hepatocyte-specific Bak/Bax double knockout (KO) mice (Sup. Fig. 3C). These results suggested that mtDNA is released from mitochondria upon apoptogenic insults in a Bak/Bax-dependent manner and further accumulates when DNase II activity is suppressed.

Increased PI-positive cells are associated with TLR9 and IFN-β activation in DNase II activity-reduced hepatocytes upon activation of the mitochondrial apoptotic pathway

Unmethylated cytidine-phosphate-guanosine (CpG) motifs on DNA, which are present on mtDNA [23], are recognized by TLR9. Hepatocytes express TLR9 [24, 25]. Activation of TLR9 induces type I IFN expression [26]. Indeed, ODN2395, a TLR9 agonist, induced type I IFN expression in CL2 cells, although it was not sufficient for activating RIP1 or reducing cell viability. (Sup.Figs.4A–4C). Thus, we hypothesized that undegraded mtDNA in DNase II activity-reduced cells activates TLR9/IFN-β signaling. We examined the mRNA expression levels of IFN-β and interferon-stimulated gene 15 (ISG15) in control and DNase II siRNA-transfected cells before and after ABT-737 treatment. mRNA expression levels of IFN-β and ISG15 did not change at baseline; however, they sharply increased in DNase II siRNA-transfected cells but not in control siRNA-transfected cells after ABT-737 treatment (Fig. 1f). To investigate the involvement of TLR9 in IFN activation and cell death, we treated DNase II-knockdown cells with

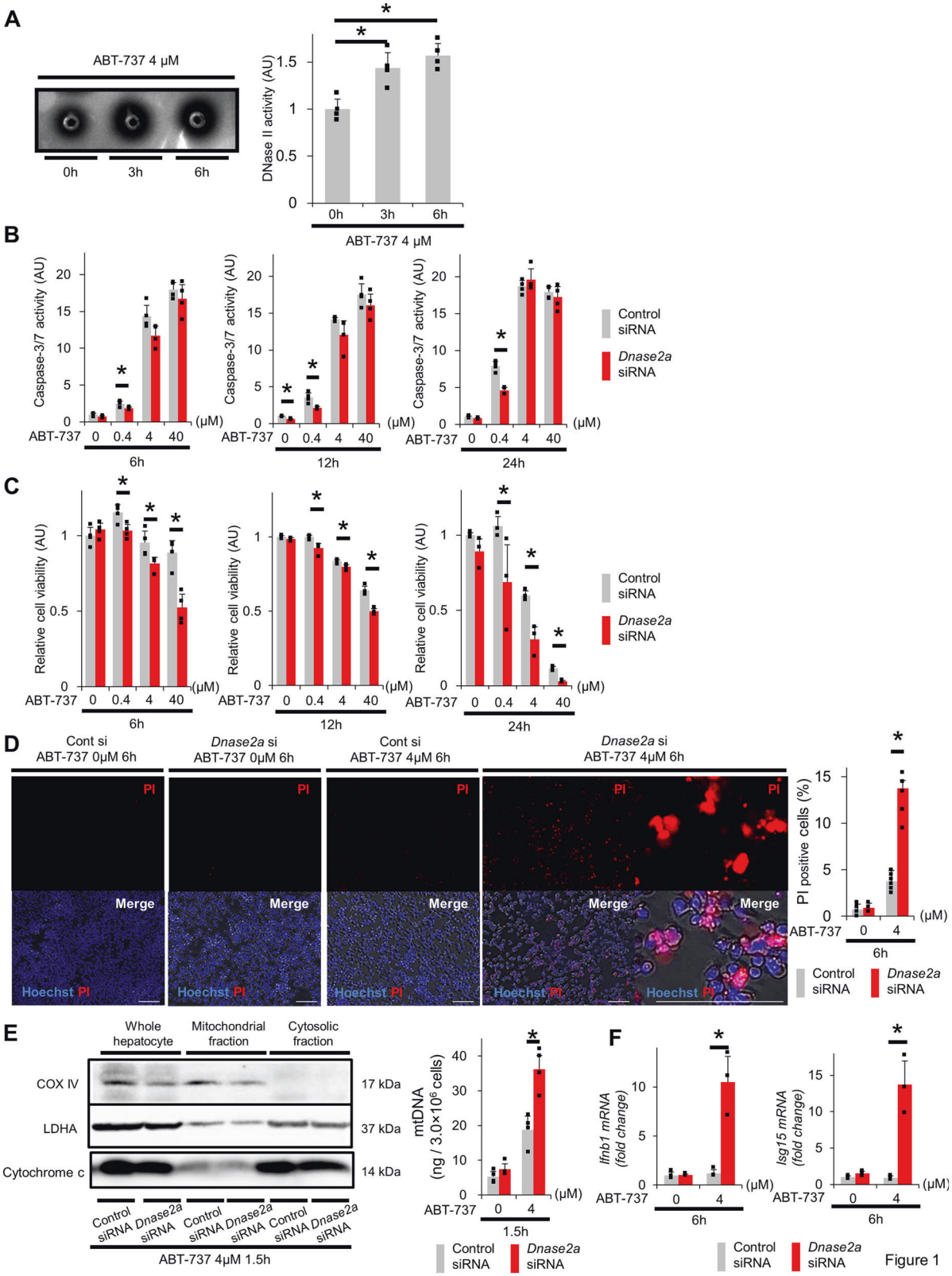

Figure 1

ODN2088, a TLR9 antagonist. Administration of ODN2088 completely abolished the ABT-737-mediated increase in IFN-β expression and suppressed ABT-737-mediated increase in PI-positive cells (Fig. 2a, b). The decrease in cell viability after ABT-737 treatment was significantly restored by ODN2088 in DNase II-knockdown

◀ **Fig. 1** ABT-737, a Bcl-xL inhibitor, induces PI-positive cells via an increase in IFN-β in cells with reduced DNase II activity. **a** BNL CL.2 cells were treated with 4 μM ABT-737 for the indicated time. DNase II activity was measured using the SRED method. Representative image and quantification of the results. **b–f** At 72 h after transfection with *Dnase2a* siRNA or control siRNA, BNL CL.2 cells were treated with 0, 0.4, 4 or 40 μM ABT-737 for the indicated time. Caspase-3/7 activity in the culture supernatant (**b**); $n = 3$–4 per group. The cell viability, assessed with a WST assay, was expressed relative to the mean of the groups treated with ABT-737 0 μM and control siRNA (**c**); $n = 3$–4. Live cell imaging via fluorescence microscopy of BNL CL.2 cells stained with PI (**d**); $n = 6$ per group. Scale bar 100 μm. Representative images and quantitative analysis. All treated cells were homogenized and were divided into cytosolic and mitochondrial fractions by centrifugation. The expression levels of the cytosolic fraction marker, LDHA, the mitochondrial fraction marker, COX IV, and cytochrome *c* were assessed by western blotting analysis (**e**, left panel). The initial quantities of cells in each lane were adjusted equally. The amount of mtDNA in the cytosolic fraction was quantified via quantitative real-time PCR for COX I (**e**, right graph); $n = 4$ per group. *Ifnb1* and *Isg15* mRNA expression levels (**f**); $n = 3$ per group. $^*P < 0.05$ based on the non-paired Student's *t*-test. Data are shown as the mean + SD

cells but was not affected in control cells (Fig. 2c). In addition, knockdown of IFN-β restored the decrease of cell viability and the increase in PI-positive cells after ABT-737 treatment in DNase II-knockdown cells (Fig. 2d, f). Next, we investigated the involvement of the cytosolic DNA sensor AIM2 in ABT-737-treated DNase II-knockdown cells. IL-1β mRNA levels were not detected in ABT-737-treated DNase II-knockdown cells (Sup.Fig.5A). siRNA-mediated AIM2 knockdown did not change caspase activity or cell viabilities in ABT-737-treated DNase II-knockdown cells compared with ABT-737-treated control cells (Sup. Fig.5D), suggesting that AIM2 is not involved with the increase in PI-positive cells after ABT-737 treatment in DNase II-knockdown cells.

Increased PI-positive cells are dependent on RIP1 but independent of caspase activation in DNase II activity-reduced hepatocytes upon activation of the mitochondrial apoptotic pathway

To characterize the PI-positive cells found in ABT-737-treated DNase II-knockdown cells, we examined necroptosis-related protein expression (Sup.Fig.6). Among ABT-737-treated or untreated DNase II-knockdown or control cells, phosphorylated RIP1 was induced only in ABT-737-treated DNase II-knockdown cells (Sup.Fig.6). We knocked down RIP1 in or administered Necrostatin-1, a specific inhibitor of RIP1, into CL2 cells. Both RIP1 knockdown and Necrostatin-1 restored cell viability and the increase in PI-positive cells without altering IFN-β expression or cytochrome *c* release after ABT-737 treatment in DNase II-knockdown cells (Fig. 2e, f, Sup.Fig.7) but did not affect control cells. ZVAD-FMK, a pan-caspase inhibitor, or Necrostatin-1 partially restored the decrease in cell viability after ABT-737 treatment in DNase II-knockdown cells, while the combination of both did it almost completely (Fig. 2g). ZVAD-FMK did not attenuate the increase in PI-positive cells or expression of IFN-β and ISG15 after ABT-737 treatment in DNase II-knockdown cells (Fig. 2h, Sup.Fig.8), suggesting PI-positive cells induced independently of caspase activation. Next, CL2 cells were treated with both ABT-737 and A-1210477, a Mcl-1 inhibitor, to examine whether this non-apoptotic death is induced even in the condition of more complete apoptosis induction. As expected, co-treatment reduced cell viability more profoundly than ABT-737 alone (Sup.Fig.9A). DNase II-knockdown increased IFN-β production and reduced cell viability in ABT-737-treated CL2 cells but did not change both of them any further in CL2 cells with co-treatment of ABT-737 and A-1210477 (Sup.Fig.9B), suggesting that non-apoptotic cell death is induced only in the condition of limited apoptosis.

Mitochondrial DNA is essential for inducing non-apoptotic cell death in DNase II activity-reduced hepatocytes upon activation of the mitochondrial apoptotic pathway

To examine the involvement of mtDNA in non-apoptotic hepatocyte death induced by ABT-737 treatment of DNase II-knockdown cells, we generated mtDNA-depleted cells via the ethidium bromide (EtBr)-mediated depletion of mtDNA [27]. Treatment with EtBr induced mtDNA depletion in CL2 cells (Fig. 3a, b). mtDNA-depleted cells proliferated at levels similar to those of wild-type cells and showed no difference in cell viability compared with that of wild-type cells (Sup.Fig.10A). Even in the mtDNA-depleted cells, treatment with ABT-737 elevated caspase-3/7 activity (Sup.Fig.10B) and reduced cell viability (Sup. Fig.10C) similar to wild-type cells (Sup.Fig.1A, Sup. Fig.1C). Furthermore, DNase II siRNA-mediated knockdown of ABT-737-treated mtDNA-depleted cells did not elevate caspase-3/7 activity (Fig. 3c) similar to wild-type cells (Fig. 1c). In contrast to the results observed in the presence of mtDNA (Fig. 1d, Sup.Fig.2D), in the mtDNA-depleted cells, DNase II siRNA-mediated knockdown of ABT-737-treated cells did not decrease cell viability (Fig. 3c, Sup.Fig.2E). Additionally, mtDNA depletion did not increase the number of PI-positive cells (Fig. 3d) or elevate the mRNA expression levels of IFN-β (Fig. 3e), unlike the results obtained in the presence of mtDNA (Figs. 1e and 2a). These results suggested that mtDNA is required for the induction of non-apoptotic death in DNase II activity-reduced cells upon activation of the mitochondrial apoptotic pathway.

Deficiency of DNase II activity in hepatocytes induces non-apoptotic death upon activation of the mitochondrial apoptotic pathway in mice

We subsequently examined the role of DNase II in hepatocytes upon activation of the mitochondrial apoptotic pathway in vivo. We previously reported that mice with a hepatocyte-specific knockout of Mcl-1 (*Mcl-1*$^{flox/flox}$ *Alb-Cre*, L-Mcl-1-KO), which is the other essential anti-apoptotic protein in hepatocytes, show spontaneous hepatocyte apoptosis [28]. Hepatocyte apoptosis in L-Mcl-1 KO mice is decreased by disrupting Bak, a mitochondrial protein, indicating that the mitochondrial apoptotic pathway is activated in the L-Mcl-1 KO mouse liver [29]. DNase II activity in L-Mcl-1-KO mouse livers was significantly higher than that in WT control littermate livers (Fig. 4a). To examine the impact of DNase II on hepatocytes in mice, we generated hepatocyte-specific DNase II-KO mice (*Dnase2a*$^{flox/flox}$ *Alb-Cre*, L-DNase II-KO). DNase II mRNA expression levels and activity were suppressed in livers from L-DNase II-KO mice (Sup.Fig.11A, Sup.Fig.11B). There were no significant differences between the L-DNase II-KO and WT mice in regard to their hematoxylin and eosin (HE)-stained liver sections, serum alanine transaminase (ALT) levels, serum caspase-3/7 activity and the number of terminal deoxynucleotidyl transferase-mediated

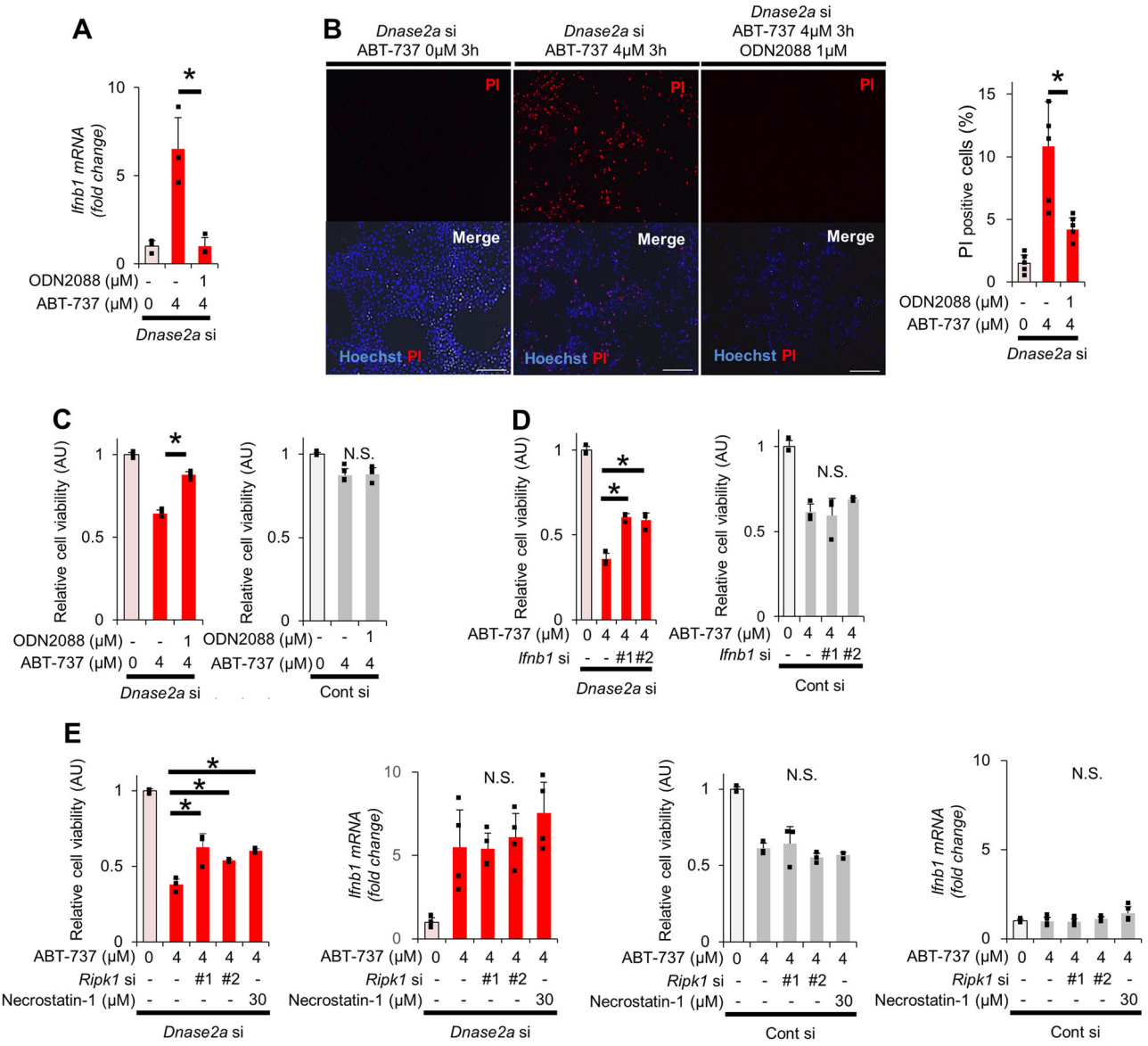

Fig. 2 (See legend on next page.)

deoxyuridine triphosphate nick-end labeling (TUNEL)-positive or PI-positive cells in their liver sections (Sup. Fig.11C-11H). We then crossed L-DNase II-KO mice with L-Mcl-1-KO mice and generated hepatocyte-specific Mcl-1/DNase II-KO (L-Mcl-1/DNase II-KO) mice. The DNase II activity in L-Mcl-1/DNase II-KO mouse livers was significantly suppressed compared with that in WT control or L-Mcl-1-KO littermate livers (Fig. 4a). Mcl-1 protein expression was reduced in L-Mcl-1/DNase II-KO mouse livers similar to that in L-Mcl-1-KO mice (Fig. 4b). The L-Mcl-1-KO and L-Mcl-1/DNase II-KO mice exhibited no significant differences in their serum caspase-3/7 activity or

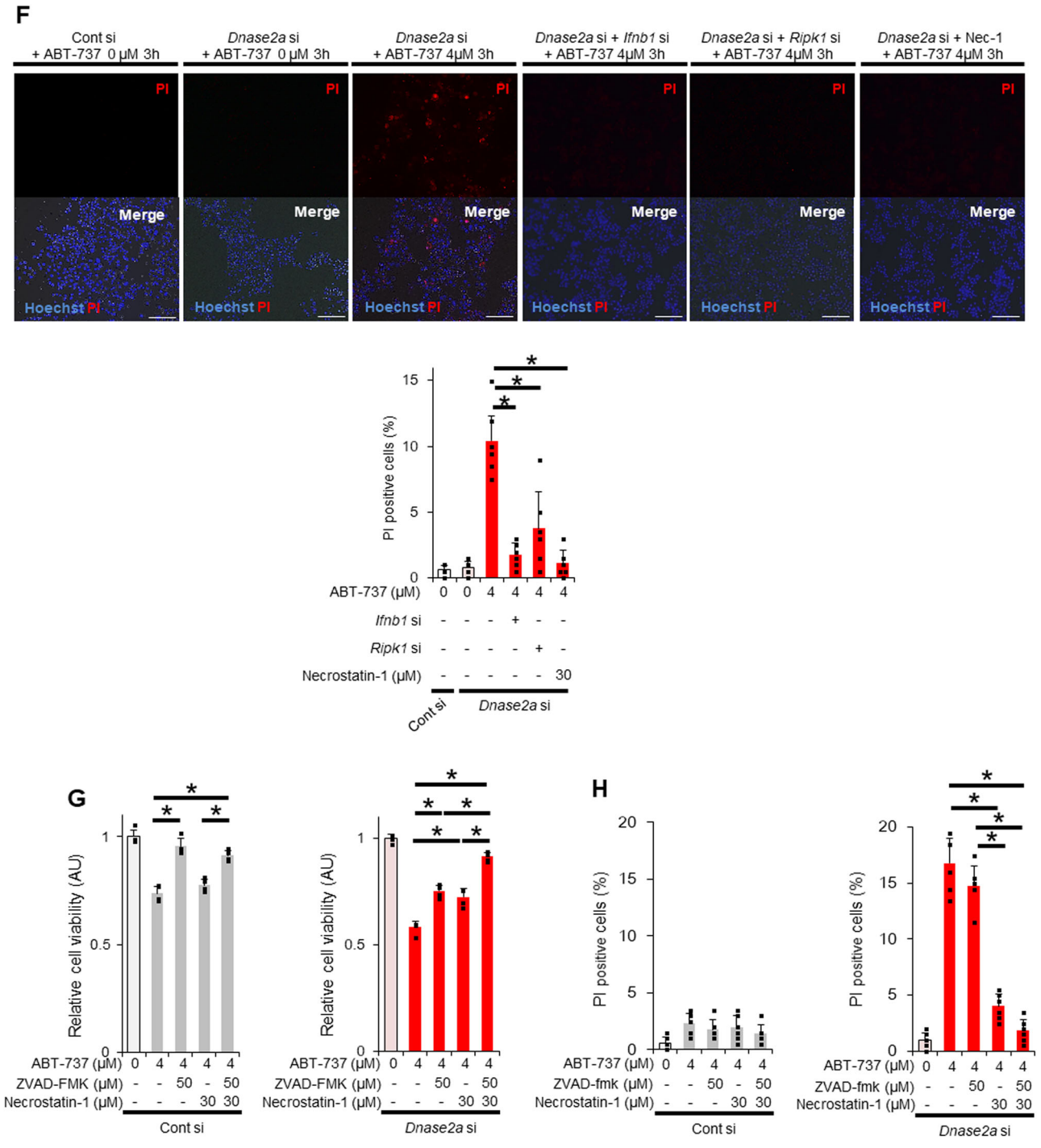

Fig. 2 (See legend on next page.)

Fig. 2 The increase in PI-positive cells among DNase II-knockdown cells treated with ABT-737 is attenuated by the inhibition of RIP1 or IFN-β but not by a pan-caspase inhibitor. At 72 h after transfection with *Dnase2a* siRNA or control siRNA, BNL CL.2 cells were treated with 0 or 4 μM ABT-737 for the indicated time. **a–c** BNL CL.2 cells were pretreated with or without ODN2088 1 h before ABT-737 treatment. *Ifnb1* mRNA expression levels after 6 h of ABT-737 treatment (**a**); $n = 4$ per group. Representative fluorescence micrographs after 3 h of ABT-737 treatment and their quantitative analysis (**b**); $n = 6$ per group. Scale bar 100 μm. Cell viability after 6 h of ABT-737 treatment, assessed with a WST assay, was expressed relative to the mean of the ABT-737 0 μM group. (**c**); $n = 4$ per group. BNL CL2 cells were co-transfected with *Infb1* siRNA (**d**, **f**) or *Ripk1* siRNA (**e**, **f**). BNL CL.2 cells were pretreated with Necrostatin-1 30 min before ABT-737 treatment (**e**, **f**). Cell viability after 6 h of ABT-737 treatment, assessed with a WST assay, was expressed relative to the mean of the ABT-737 0 μM group. (**d**, **e**); $n = 3$ - 4 per group. Representative fluorescence micrographs after 3 h of ABT-737 treatment and their quantitative analysis (**f**); $n = 6$ per group. Scale bar 100 μm. (**g, h**) BNL CL.2 cells were pretreated with Necrostatin-1 and/or ZVAD-FMK 30 min before ABT-737 treatment for 6 h. BNL CL.2 cells were pretreated with Necrostatin-1 and/or ZVAD-FMK 30 min before ABT-737 treatment for 6 h. The cell viability was expressed relative to the mean of the ABT-737 0 μM group (**g**). Live cell imaging via fluorescence microscopy of BNL CL.2 cells stained with PI (**h**); n = 6 per group. Quantitative analysis. In each analysis, the ABT-737 0 μM group was used as a reference (**a–h**). N.S. not significant. Data are shown as the mean + SD. $^*P < 0.05$ based on the non-paired Student's t-test

number of TUNEL-positive hepatocytes (Fig. 4c, d). In contrast, the number of PI-positive cells in livers from L-Mcl-1/DNase II-KO mice was significantly greater than that in livers from L-Mcl-1-KO mice (Fig. 4e). The serum ALT levels and IL-1α levels of L-Mcl-1/DNase II-KO mice were significantly higher than those of L-Mcl-1-KO mice (Fig. 4c). In addition, the amount of mtDNA isolated from the cytosolic fraction of L-Mcl-1/DNase II-KO mouse livers was also significantly higher than that from L-Mcl-1-KO mouse livers (Fig. 4f).

Non-apoptotic hepatocyte death in L-Mcl-1/DNase II-KO mice depends on TLR9/IFN-β signaling and RIP1

To investigate the mechanisms underlying the induction of non-apoptotic hepatocyte death in L-Mcl-1/DNase II-KO mice, we examined the TLR9/IFN-β signaling pathway based on our in vitro results. The mRNA expression levels of IFN-β and ISG15, but not IL-1β, were elevated in the livers of L-Mcl-1/DNase II-KO mice compared with the levels in livers of L-Mcl-1-KO mice (Fig. 4f, Sup.Fig.5B). We performed a complementary DNA microarray analysis using total RNA from the livers of L-Mcl-1-KO and L-Mcl-1/DNase II-KO mice. According to the pathway analysis, IFN-β is one of the top upstream regulators (Sup.Table1), which supported the involvement of TLR9/IFN-β signaling in the induction of non-apoptotic hepatocyte death in L-Mcl-1/DNase II-KO mice. The administration of ODN2088, a TLR9 antagonist, decreased the serum ALT levels in L-Mcl-1/DNase II-KO mice but not in L-Mcl-1-KO mice (Fig. 5a). After the administration of ODN2088, the number of PI-positive hepatocytes was also decreased (Fig. 5b), and the increased mRNA expression of IFN-β in L-Mcl-1/DNase II-KO mouse livers was attenuated (Fig. 5c). The administration of Necrostatin-1 also attenuated the serum ALT levels and the number of PI-positive hepatocytes in L-Mcl-1/DNase II-KO mice but not in L-Mcl-1 KO mice (Fig. 5d, e).

HFD decreases DNase II activity and increases non-apoptotic hepatocyte death

Research has shown that WT mice fed the HFD exhibit increased hepatocyte apoptosis in a time-dependent manner [30]. We examined DNase II activity in livers from WT mice fed the HFD for 8 months and found it was reduced compared with the activity in livers from WT mice fed a normal diet (ND) (Fig. 6a). Compared with mice fed the ND, WT mice fed the HFD for 8 months exhibited an increased number of TUNEL-positive cells as well as cleaved caspase-3-positive cells in liver sections (Fig. 6b), indicating increased hepatocyte apoptosis. Importantly, WT mice fed the HFD showed a significantly increased number of PI-positive cells (Fig. 6c) and significantly increased IFN-β expression (Fig. 6d). To examine the role of DNase II in the livers of HFD models, we fed WT mice and L-DNase II-KO mice the ND or HFD and analyzed the phenotypes of WT mice and L-DNase II-KO mice fed the HFD for 8 months (Fig. 6a). The number of TUNEL-positive cells or cleaved caspase-3-positive cells in the liver sections did not change with the disruption of DNase II in hepatocytes (Fig. 6b). In contrast, the number of PI-positive cells and the mRNA expression levels of IFN-β in the liver significantly increased (Fig. 6c, d). The serum ALT levels were significantly higher in the L-DNase II-KO mice than in the WT mice (Fig. 6e). Liver fibrosis was exacerbated in the L-DNase II-KO mice compared with that in the WT mice, as evidenced by Sirius Red staining and the mRNA expression levels of Col1a2 in the liver (Fig. 6b, d). These results indicate that hepatocyte DNase II regulates the development of non-apoptotic hepatocyte death and the progression of fibrosis in the liver of HFD models. Taken together, these results suggest that the decrease in DNase II activity observed in HFD models is involved in the development and progression of steatohepatitis.

Discussion

Chronic liver diseases include various types of cell death such as apoptosis and necrotic cell death [22]. NASH is

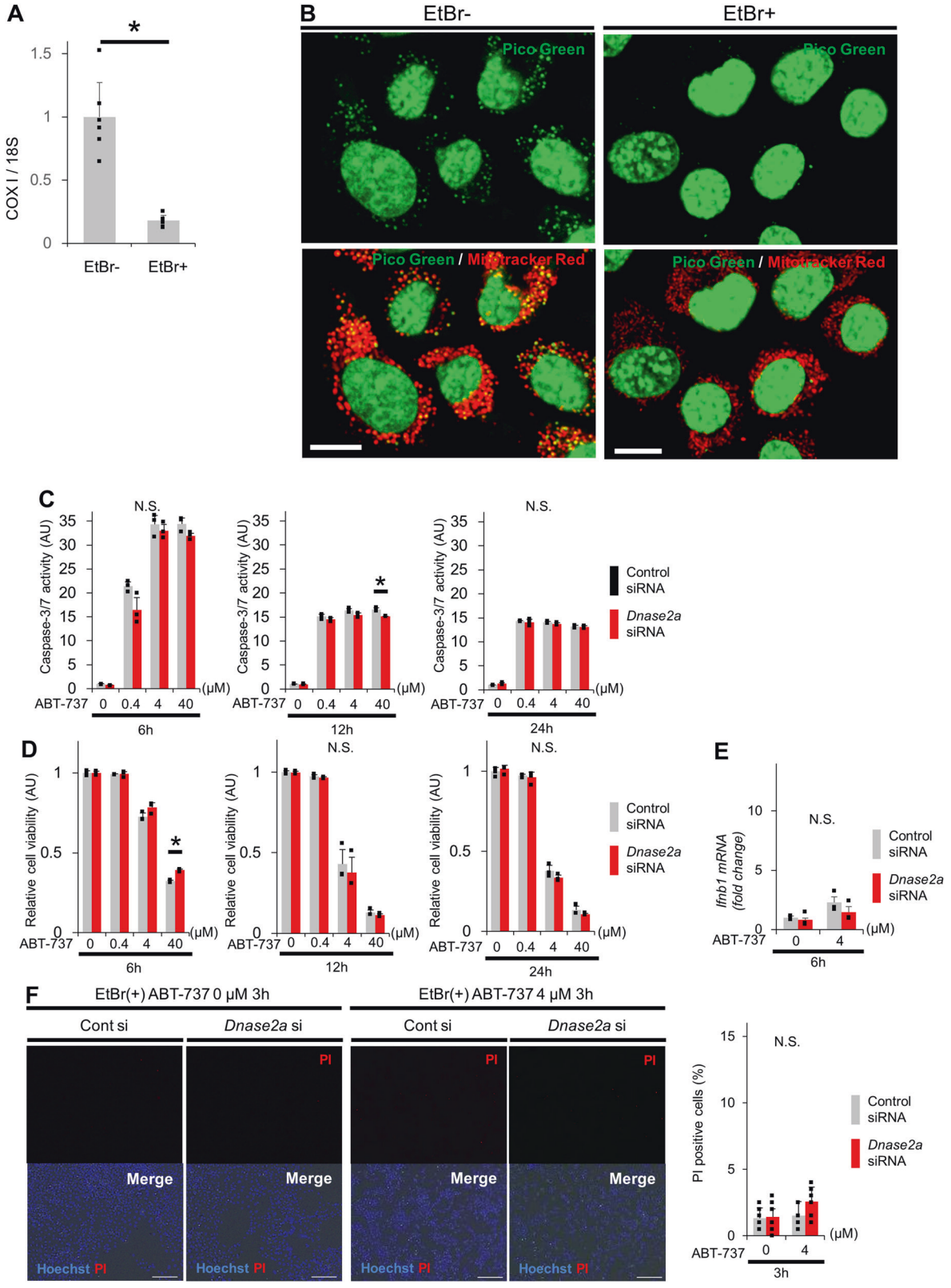
A
COX I / 18S
EtBr-
EtBr+
B
EtBr-
EtBr+
Pico Green
Pico Green / Mitotracker Red
C
Caspase-3/7 activity (AU)
N.S.
ABT-737 0 0.4 4 40 (μM)
6h
12h
24h
Control siRNA
Dnase2a siRNA
D
Relative cell viability (AU)
E
Ifnb1 mRNA (fold change)
F
EtBr(+) ABT-737 0 μM 3h
EtBr(+) ABT-737 4 μM 3h
Cont si
Dnase2a si
PI
Merge
Hoechst PI
PI positive cells (%)
3h

◀ **Fig. 3** In the absence of mtDNA, activation of the mitochondrial apoptosis pathway by ABT-737 in BNL CL.2 cells with reduced DNase II activity does not induce non-apoptotic death. **a**, **b** BNL CL.2 cells were cultured with DMEM containing 200 ng/ml ethidium bromide (EtBr) with 10% FBS for 4 days and then analyzed. The ratio of the mtDNA copy number normalized to chromosomal DNA was quantified via quantitative real-time PCR for COX I and 18S ribosomal RNA (18S); $n = 6$ per group (**a**). Live cell imaging of BNL CL.2 cells stained with PicoGreen to detect mtDNA (**b**). Representative images. Scale bar 10 μm. **c**–**f** After depletion of mtDNA, BNL CL.2 cells were transfected with *Dnase2a* siRNA or control siRNA. At 72 h after transfection, these cells were treated with 0, 0.4, 4 or 40 μM ABT-737 for the indicated time. Caspase-3/7 activity in the culture supernatant (**c**). The cell viability, assessed with a WST assay, was expressed relative to the mean of the groups treated with ABT-737 0 μM and control siRNA (**d**); $n = 3$ per group. *Ifnb1* mRNA expression levels; $n = 3$ per group (**e**). Live cell imaging via fluorescence microscopy of BNL CL.2 cells stained with PI to detect necrotic cells; $n = 6$ per group. Scale bar 100 μm (**f**). Representative images and their quantitative analysis. N.S. not significant. Data are shown as the mean + SD. $^*P < 0.05$ based on the non-paired Student's *t*-test

characterized by both hepatocyte apoptosis [14, 15] and necrosis [18, 19]. In general, each different mode of cell death is considered to be induced by different stimuli. Here, we show that DNase II activity is elevated upon activation of the mitochondrial apoptotic pathway and that suppression of DNase II activity upon activation of the mitochondrial apoptotic pathway induces RIP1-dependent non-apoptotic hepatocyte death through the TLR9/IFN-β pathway. These findings suggest that apoptotic stimuli have the ability to induce RIP1-dependent cell death with necrotic phenotype and reveal a potential link between apoptosis and necrosis under the suppression of DNase II activity. In livers from the HFD-fed mice in the present study, DNase II activity was suppressed. This reduced DNase II activity may contribute to the induction of hepatocyte necrosis in NASH and could affect the exacerbation of NASH.

The liver is a mitochondrion-rich organ, and mitochondria contain many DAMPs, including mtDNA, formyl peptides, cytochrome *c* and adenosine triphosphate [31]. mtDNA is released into the cytosol upon activation of the mitochondrial apoptotic pathway [9, 10]. DNA in the cytosol can be directly uptaken to lysosomes by SID1 transmembrane family member 2 (SIDT2) [32]. In the present study, apoptogenic insults via the simple inactivation of Bcl-xL by ABT-737 increased the amount of cytosolic mtDNA, which further accumulated in DNase II-knockdown cells. Cytosolic DNA is recognized by cytosolic receptors, including TLRs and cyclic-GMP-AMP synthase (cGAS), and induces type I IFN [33, 34]. mtDNA contains unmethylated CpG motifs [23], and CpG DNA is recognized by TLR9 [33]. In the present study, the non-apoptotic hepatocyte death induced in DNase II activity-reduced cells upon activation of the mitochondrial pathway was dependent on mtDNA, and it was attenuated by treatment with the TLR9 antagonist ODN2088. Thus, recognition of mtDNA by TLR9 is involved in the mechanism underlying non-apoptotic cell death induction. Activation of the TLR9/IFN-β pathway is required, but not sufficient for the execution of this type of cell death, because TLR9 agonist efficiently induced IFN-β in hepatocytes but did not decrease cell viability. Further study is needed to clarify whether mtDNA recognized via TLR9 comes from its own cells or neighboring cells.

Compatible with in vitro results, the amount of cytosolic mtDNA in L-Mcl-1/DNase II-KO mouse livers increased compared with that in L-Mcl-1 KO mouse livers. The non-apoptotic hepatocyte death observed in L-Mcl-1/DNase II-KO mouse livers was attenuated by treatment with the TLR9 antagonist ODN2088. Garcia-Martinez et al. [35] reported high levels of hepatocyte mtDNA in plasma from mice and patients with NASH. However, the impact of intracellular mtDNA in NASH remains to be elucidated. In the present study, suppressed DNase II activity and non-apoptotic hepatocyte death with increased expression of IFN-β were observed in HFD-fed WT mice. Further reduction in DNase II activity exacerbated non-apoptotic hepatocyte death and promoted fibrosis in HFD-fed mouse livers. Taken together, these results suggest that undegraded intracellular mtDNA is involved in non-apoptotic hepatocyte death, which contributes to the progression of NASH.

In this study, our results showed that DNase II activity in the liver was compromised in mice fed the HFD despite the clear activation of hepatocyte apoptosis. This finding is clearly different in that pure activation of the mitochondrial apoptosis pathway by inactivation of Bcl-xL or Mcl-1 increased DNase II activity. The underlying mechanism by which DNase II activity is suppressed in fatty livers remains unclear. We previously reported that HFD induces impairment of autophagy [30], and Inami et al. [36] reported that lipid accumulation reduces lysosomal acidity, suggesting inhibition of autophagic flux. In addition, DNase II activity is exerted in acidic environments because DNase II is an acid DNase [12]. Therefore, the dysregulation of lysosomal acidification in fatty livers might contribute to reduced DNase II activity. Further experiments are needed to clarify the mechanism underlying the reduction in DNase II activity.

In the present study, we showed that mtDNA released from mitochondria activates IFN-β in DNase II activity-reduced cells, leading to induction of non-apoptotic cell death. While ABT-737-mediated mtDNA release was dependent on Bak and Bax, neither the IFN-β activation nor non-apoptotic cell death induction was blocked by a pan-caspase inhibitor, suggesting that ABT-737-induced IFN-β production and non-apoptotic cell death in DNase II activity-reduced cells was dependent on Bak/Bax activation but independent of caspase activity. On the other hand,

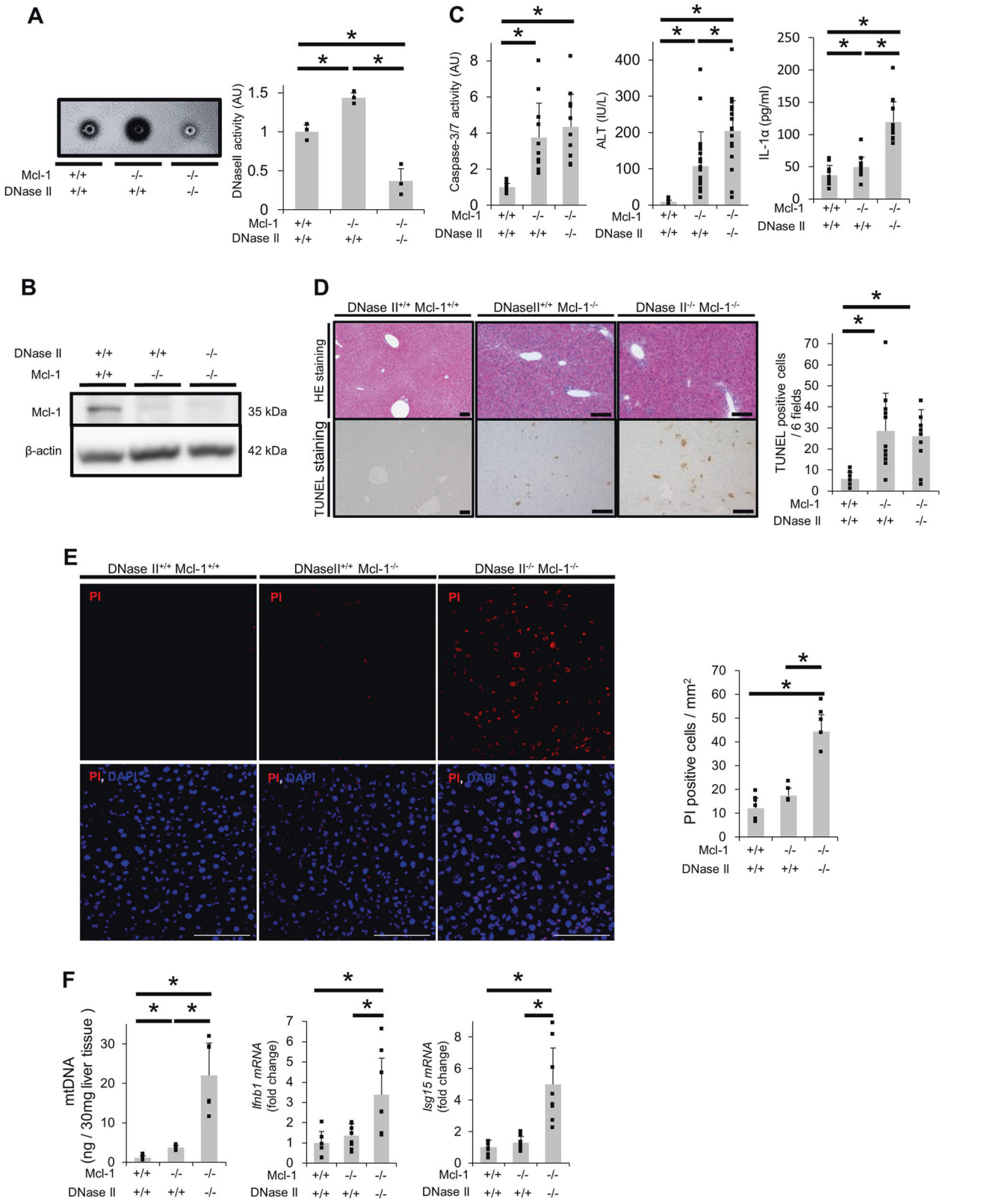
A
Mcl-1 +/+ -/- -/-
DNase II +/+ +/+ -/-
DNaseII activity (AU)
B
DNase II +/+ +/+ -/-
Mcl-1 +/+ -/- -/-
Mcl-1
β-actin
35 kDa
42 kDa
C
Caspase-3/7 activity (AU)
ALT (IU/L)
IL-1α (pg/ml)
D
DNase II+/+ Mcl-1+/+
DNaseII+/+ Mcl-1-/-
DNase II-/- Mcl-1-/-
HE staining
TUNEL staining
TUNEL positive cells / 6 fields
E
PI
PI, DAPI
PI positive cells / mm2
F
mtDNA (ng / 30mg liver tissue)
Ifnb1 mRNA (fold change)
Isg15 mRNA (fold change)

◀ **Fig. 4** Deficiency in hepatocyte DNase II in L-Mcl-1-KO mice increased non-apoptotic hepatocyte death but not hepatocyte apoptosis. We mated *Mcl-1*$^{flox/flox}$ *Dnase2a*$^{flox/+}$ *Alb-Cre* mice and *Mcl-1*$^{flox/flox}$ *Dnase2a*$^{flox/+}$ mice and generated L-Mcl-1-KO mice, L-Mcl-1/DNase II-KO mice and control littermates (*Mcl-1*$^{flox/flox}$ *Dnase2a*$^{any/any}$). The littermates were analyzed at 6 to 8 weeks of age; $n \geq 8$ per group unless otherwise indicated. **a** DNase II activity in whole livers was measured using the SRED method. Representative figures and graphs of the quantitative results; $n = 3$ per group. **b** Expression of Mcl-1 and β-actin proteins assessed by western blotting analysis of liver lysates. **c** Serum caspase-3/7 activity, serum ALT levels and serum IL-1α levels. **d** HE and TUNEL staining of liver sections. Representative images and the quantitative results of TUNEL-positive cell counts. **e** Confocal micrographs of PI-injected mouse livers. Representative images and the quantitative results of PI-positive cell counts; $n = 4$–6 per group. Scale bar 100 μm. **f** The amount of mtDNA in cytosolic fractions was quantified via quantitative real-time PCR for COX I; $n = 6$ per group (left graph). *Ifnb1* and *Isg15* mRNA expression levels; $n = 8$ per group (middle and right graphs). Data are shown as the mean + SD. $^*P < 0.05$ based on one-way ANOVA followed by Tukey's HSD test

study reported that mtDNA released into the cytoplasm of apoptotic cells is not capable of inducing IFN production when caspases are active [9, 10]. In the present study, we did not find any difference in caspase activity between control cells and DNase II activity-reduced cells and, therefore IFN production and resultant non-apoptotic cell death seems to occur even if caspases are active. In the previous reports, they used hematopoietic cells or mouse embryonic fibroblasts, but not hepatocytes, in their experiments [9, 10]. The difference of cell types may cause the difference of caspase dependency in IFN-β production. Another possibility is that levels of caspase activity are diverse in cells and that cells with low caspase activity might be more prone to IFN production in our experiments. In condition of full Bak/Bax activation with both ABT-737 and A-1210477, a Mcl-1 inhibitor, there was no difference in IFN-β production or cell viability between DNase II activity-reduced cells and unreduced cells, suggesting that mtDNA/IFN-β-induced non-apoptotic cell death is only apparent under conditions of limited apoptosis which may admit diversity of caspase activity. However, in the condition of limited apoptosis which might be more significant in pathological conditions, mtDNA released from mitochondria has to be degraded by DNase II to avoid further destruction of cells via non-apoptotic cell death. Additionally, cells with minority MOMP [37], where minority of mitochondria develop MOMP and fail to induce apoptosis, might be involved in activation of IFN-β or induction of non-apoptotic cell death in DNase II activity-reduced cells. Further analysis at single cell level will be needed for clarifying detail mechanisms by which non-apoptotic death is induced in DNase II activity-reduced cells upon activation of the mitochondrial apoptotic pathway.

In conclusion, a lack of DNase II in hepatocytes induces RIP1-dependent non-apoptotic cell death with necrotic phenotype through the mtDNA-driven activation of TLR9/IFN-β signaling pathway upon activation of the mitochondrial apoptotic pathway. Our results describe the mechanism of a potential relationship between hepatocyte apoptosis and necrosis and have implications for understanding the progression of chronic liver disease. Reduced DNase II activity might induce mtDNA-driven non-apoptotic cell death, especially in the pathogenesis of NASH, and could be one of the potential mechanisms involved in its progression.

Materials and methods

Cells and reagents

The murine hepatocyte cell line, BNL CL.2s cell, was obtained from the American Type Culture Collection (ATCC, Manassas, VA, USA). The cells were cultured in Dulbecco's modified Eagle's medium (DMEM; Sigma-Aldrich, St. Louis, MO, USA) supplemented with 10% fetal bovine serum at 37 °C under 5% CO_2. ABT-737 was kindly provided by AbbVie (North Chicago, IL, USA). In some experiments, the cells were pretreated with a TLR9 agonist, ODN2395, or a TLR9 antagonist, ODN2088 (InvivoGen, San Diego, CA, USA), at 1 μM, the RIP1 inhibitor, Necrostatin-1 (Calbiochem, San Diego, CA, USA), at 30 μM or ZVAD-FMK (Calbiochem) at 50 μM, for the indicated time and were then reacted with specific media for further investigation as indicated. All in vitro experiments were repeated at least two or three times.

Mice

C57BL/6J mice (WT mice) were purchased from Charles River Japan (Tokyo, Japan). We crossed mice bearing the *Dnase2a*^{flox} allele [38] with *Alb-Cre* transgenic mice expressing Cre recombinase under the control of the albumin gene promoter, generating hepatocyte-specific DNase II-KO mice (*Dnase2a*$^{flox/flox}$ *Alb-Cre*). We previously reported hepatocyte-specific Mcl-1-KO (L-Mcl-1-KO) mice, which spontaneously undergo continuous hepatocyte apoptosis [28]. Hepatocyte-specific Mcl-1/DNase II-KO (*Mcl-1*$^{flox/flox}$ *Dnase2a*$^{flox/flox}$ *Alb-Cre*) mice (L-Mcl-1/DNase II-KO mice) were generated by crossing L-DNase II-KO mice and L-Mcl-1-KO mice. The TLR9 antagonist ODN2088 was administered intraperitoneally (50 μg/200 μl) for 2 consecutive days, and Necrostatin-1 was administered intraperitoneally (6 mg/kg) once. In some experiments, male mice aged 6–8 weeks were fed the HFD containing 32% fat (HFD32; CLEA Japan, Tokyo, Japan) or the ND containing 5% fat (CRF-1; CLEA Japan) for 8 months. All mice were housed in a specific pathogen-free facility and treated with humane care. The animal care and use committee at Osaka University Medical School approved all of the experiments.

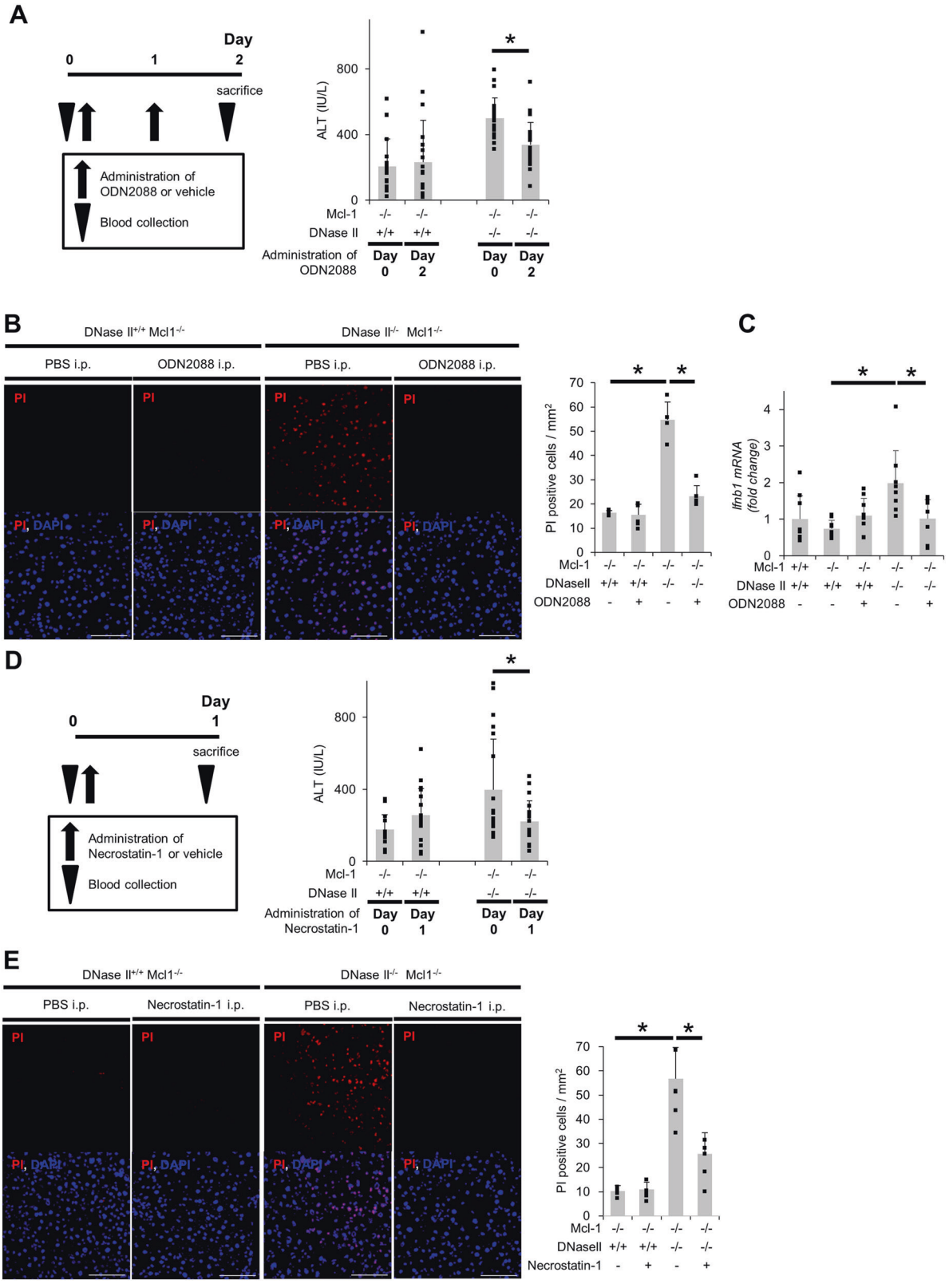
A
Day
0
1
2
sacrifice
Administration of ODN2088 or vehicle
Blood collection
ALT (IU/L)
800
400
0
*
Mcl-1 -/- -/- -/- -/-
DNase II +/+ +/+ -/- -/-
Administration of ODN2088 Day 0 Day 2 Day 0 Day 2
B
DNase II+/+ Mcl1-/-
DNase II-/- Mcl1-/-
PBS i.p.
ODN2088 i.p.
PI
PI, DAPI
PI positive cells / mm2
70
60
50
40
30
20
10
0
Mcl-1 -/- -/- -/- -/-
DNaseII +/+ +/+ -/- -/-
ODN2088 - + - +
C
Ifnb1 mRNA (fold change)
4
3
2
1
0
Mcl-1 +/+ -/- -/- -/- -/-
DNase II +/+ +/+ +/+ -/- -/-
ODN2088 - - + - +
D
Day
0
1
sacrifice
Administration of Necrostatin-1 or vehicle
Blood collection
ALT (IU/L)
800
400
0
Mcl-1 -/- -/- -/- -/-
DNase II +/+ +/+ -/- -/-
Administration of Necrostatin-1 Day 0 Day 1 Day 0 Day 1
E
DNase II+/+ Mcl1-/-
DNase II-/- Mcl1-/-
PBS i.p.
Necrostatin-1 i.p.
PI
PI, DAPI
PI positive cells / mm2
70
60
50
40
30
20
10
0
Mcl-1 -/- -/- -/- -/-
DNaseII +/+ +/+ -/- -/-
Necrostatin-1 - + - +

◀ **Fig. 5** Hepatocyte non-apoptotic cell death in L-Mcl-1/DNase II-KO mice is induced by TLR9/IFN-β signaling and is dependent on RIP1. L-Mcl-1-KO mice, L-Mcl-1/DNase II-KO mice and control littermates (*Mcl-1*$^{flox/flox}$ *Dnase2a*$^{any/any}$) at 6 to 8 weeks of age were intraperitoneally treated with ODN2088, Nec-1 or vehicle. Schematic of the experimental procedure for the continuous collection of blood samples and serum ALT levels at the indicated times (**a**, **d**); $n = 20$ per group. Confocal micrographs of PI-injected L-Mcl-1-KO and L-Mcl-1/DNase II-KO mouse livers. Representative images and their quantitative analysis; $n = 4$–6 per group. Scale bar 100 μm (**b**, **e**). *Ifnb1* mRNA expression levels; $n = 7$–8 per group (**c**). N.S. not significant. $^*P < 0.05$ based on paired Student's *t*-test for (**a**, **d**) and one-way ANOVA followed by Tukey's HSD test for (**b**, **c**, **e**)

Measurement of DNase II activity

DNase II activity was measured with the single radial enzyme-diffusion (SRED) method, which can measure the activity of DNase II, but not DNase I, phosphodiesterase I or phosphodiesterase II [39, 40]. Equivalent amounts of cultured cells or liver homogenates, normalized based on their protein concentrations, were applied to wells with radii of 1.5 mm that were punched in a 1% (w/v) agarose gel containing 0.05 mg/ml salmon sperm DNA (Sigma-Aldrich), 5 μg/ml EtBr (Nakalai Tesque, Kyoto, Japan), 0.5 M sodium acetate buffer (pH 4.7) and 10 mM EDTA. The radii of the dark circles were measured under ultraviolet light after 24–72 h of incubation at 37 °C. To determine the DNase II activity of the samples, a standard curve was constructed using porcine DNase II (Sigma-Aldrich).

In vitro and in vivo evaluation of hepatocyte death and histological analysis

Cell viability was assessed with a water-soluble tetrazolium salt (WST) assay (Nakalai Tesque) and/or by counting viable cells automatically (TC20 Cell Counter, Bio-Rad, Hercules, CA, USA) after Trypan blue staining. In some experiments, BNL CL.2 cells were treated with A-1210477, an Mcl-1 inhibitor (MCE Monmouth Junction, NJ, USA). L-929 cells, murine fibroblast cell line, were pretreated with 50 μM ZVAD for 30 min and then treated with 20 ng/ml recombinant mouse tumor necrosis factor-α for 1.5 h. Mouse serum ALT levels were measured using a standard method at the Oriental Kobo Life Science Laboratory (Nagahama, Japan). Mouse serum IL-1α levels were measured by enzyme-linked immunosorbent assay (ELISA) kit (LSBio, Seattle, WA, USA) according to the manufacturer's protocol. For apoptosis assays, the supernatant of cultured cells or mouse serum was measured with a luminescent substrate assay for caspase-3 and caspase-7 (Caspase-Glo Assay, Promega, Madison, WI, USA) according to the manufacturer's protocol. TUNEL staining was performed using an ApopTag Kit (Millipore, Moldheim, France) according to the manufacturer's protocol. For immunohistochemical staining, cleaved caspase-3 was labeled in paraffin-embedded liver sections using cleaved caspase-3 antibody (#9661, Cell Signaling Technology, Beverly, MA, USA). Bound primary antibody was detected with avidin-biotin complexes using a Vectastain ABC Kit (Vector Laboratories, Burlingame, CA, USA). TUNEL-positive cells and cleaved caspase-3-positive cells were counted in six fields per liver section at 100× magnification. CL2 cells were stained with 5 μg/ml PI for 15 min and then washed three times with phosphate-buffered saline (PBS). Live cells were analyzed with a BZ-9000 or BZ-X700 fluorescence microscope (KEYENCE, Osaka, Japan). The percentage of PI-positive cells was calculated by counting more than 200 cells on each dish. PI (5 mg/kg per mouse) (WAKO, Osaka, Japan) was injected into mice via the tail vein 1 h before killing. The mouse livers were subsequently collected and cryopreserved with a cryopreservation compound. Cryosections from the mouse livers were analyzed with an FV1000D confocal microscope (Olympus, Tokyo, Japan). PI-positive cells were counted in six fields per liver section. Liver fibrosis was evaluated with Sirius Red staining. The Sirius Red-positive area was measured with ImageJ software (National Institute of Health, Bethesda, MD, USA).

siRNA-mediated knockdown

siRNAs for *Dnase2a* (s65051, s65055), *Ifnb1* (s68092, s201518), *Ripk1* (s72976, s72977), *Aim2* (s234106, s234107) and the appropriate negative controls were purchased from Thermo Fisher Scientific (Waltham, MA, USA). CL2 cells were transfected with 5 nM siRNA using Lipofectamine RNAiMAX (Invitrogen) according to the manufacturer's protocol. At 72 h after transfection, CL2 cells were analyzed or treated with ABT-737 unless otherwise indicated.

Quantitative real-time RT-PCR analysis

Total RNA extracted from cells and livers with an RNeasy Kit (QIAGEN) was reverse-transcribed using ReverTra Ace qPCR RT Master Mix (TOYOBO, Osaka, Japan). Real-time reverse transcription polymerase chain reaction (RT-PCR) was performed using TaqMan Gene Expression Assays with an HT7900 Fast Real-Time PCR System (Applied Biosystems, Thermo Fisher Scientific). The following primer probes were used: *Dnase2a* (Mm00438463_m1), *Col1a2* (Mm01165187_m1), *Ifna4* (Mm00833969_s1), *Ifnb1* (Mm00439552_s1), *Isg15* (Mm01705338_s1), *Actb* (Mm02619580_g1) and *Il-1b* (Mm00434228_m1). Gene expression was normalized to *Actb*.

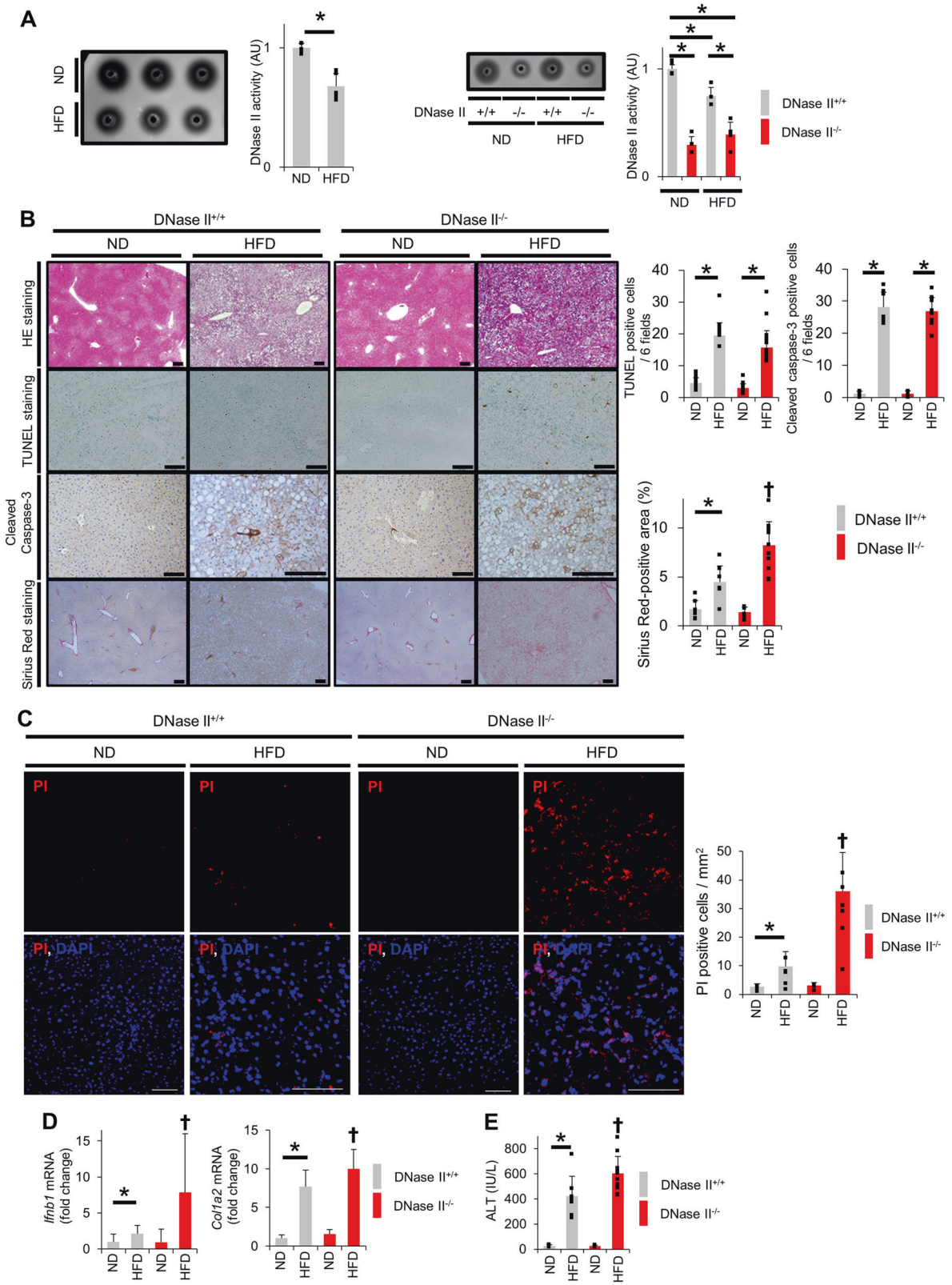
A
ND
HFD
DNase II activity (AU)
ND HFD
DNase II +/+ -/- +/+ -/-
ND HFD
DNase II activity (AU)
DNase II+/+
DNase II-/-
B
DNase II+/+
DNase II-/-
ND HFD ND HFD
HE staining
TUNEL staining
Cleaved Caspase-3
Sirius Red staining
TUNEL positive cells / 6 fields
Cleaved caspase-3 positive cells / 6 fields
Sirius Red-positive area (%)
DNase II+/+
DNase II-/-
C
DNase II+/+
DNase II-/-
ND HFD ND HFD
PI
PI, DAPI
PI positive cells / mm2
DNase II+/+
DNase II-/-
D
Ifnb1 mRNA (fold change)
Col1a2 mRNA (fold change)
DNase II+/+
DNase II-/-
E
ALT (IU/L)
DNase II+/+
DNase II-/-

◀ **Fig. 6** HFD feeding reduces hepatocyte DNase II activity and increases hepatocyte non-apoptotic cell death. **a** C57BL/6J mice, L-DNase II-KO mice and their WT littermates were fed the HFD or ND for 8 months. DNase II activity in liver homogenates from C57BL/6J mice was measured using the SRED method; $n = 5$ per group (left panel). Representative image and quantitative analysis. The DNase II activity in liver homogenates from L-DNase II-KO mice and their WT littermates was measured using the SRED method; $n = 5$ per group (right panel). Representative image and quantitative analysis. **b–e** L-DNase II-KO mice and WT littermates fed the HFD or ND for 8 months were analyzed. HE staining, TUNEL staining, immunohistochemical staining of cleaved caspase-3 and Sirius Red staining of liver sections; $n \geq 6$ per group (**b**). Representative images of stained sections and their quantitative analysis. Confocal micrographs of PI-injected mouse liver sections; $n = 3$–6 per group. Scale bar 100 μm (**c**). Representative images and their quantitative analysis. *Ifnb1* and *Col1a2* mRNA expression levels; $n \geq 6$ per group (**d**). Serum ALT levels; $n \geq 6$ per group (**e**). $^{\dagger}P < 0.05$ vs the other groups and $^{*}P < 0.05$ based on one-way ANOVA followed by Tukey's HSD test. ND normal diet, HFD high-fat diet

Measurement of mtDNA in the cytosolic fraction

To determine the amount of mtDNA in the cytosol, 3.0×10^6 cells from the in vitro assays or 30 mg wet weight of liver tissue were homogenized with a Dounce homogenizer in 100 mM Tricine-NaOH solution, pH 7.4, containing 0.25 M sucrose, 1 mM EDTA and protease inhibitor, and the homogenates were centrifuged at $700 \times g$ for 10 min at 4 °C. After normalization of their protein concentrations, the supernatants were centrifuged at $10{,}000 \times g$ for 30 min at 4 °C. The resulting supernatants and pellets were defined as the cytosolic and mitochondrial fractions, respectively [41]. The distribution of these fractions was assessed by western blotting for lactate dehydrogenase A (LDHA), a cytosolic fraction marker, and cytochrome *c* oxidase IV (COX IV), a mitochondrial fraction marker. DNA was isolated from 200 μl of the cytosolic fraction using a DNeasy Blood and Tissue Kit (QIAGEN). The amount of mtDNA was quantified via quantitative real-time PCR using primers for COX I: forward, 5'-CCCCAGATATAGCATTCCC-3', and reverse, 5'-GTTCATCCTGTTCCTGCTCC-3'. To construct the standard curve, mitochondria were isolated from C57BL/6J mouse livers using a Mitochondrial Isolation Kit for Tissue (Thermo Fisher Scientific), and mtDNA was extracted from the isolated mitochondria using a DNeasy Blood and Tissue Kit (QIAGEN).

Depletion of mtDNA

BNL CL.2 cells were cultured with DMEM containing 200 ng/ml EtBr with 10% FBS for 4 days [27, 41]. The cells were then cultured and reacted with specific medium without EtBr for further investigations as indicated. To measure the efficiency of mtDNA depletion, total DNA was extracted by resuspending these cells in 50 mM NaOH at 95 °C for 1 h, followed by neutralization through the addition of a 10% volume of 1 M Tris HCl (pH 8.0). mtDNA and chromosomal DNA were quantified via quantitative real-time PCR using the primers for COX I described above, as well as primers for 18S ribosomal RNA: forward, 5'-TAGAGGGACAAGTGGCGTTC-3', and reverse, 5'-CGCTGAGCCAGTCAGTGT-3'. The mtDNA copy number was normalized to the chromosomal DNA and compared with that of untreated cells to calculate the percentage of depletion. PicoGreen (Molecular Probes, Thermo Fisher Scientific) was used to detect mtDNA [42] under live cell imaging according to the manufacturer's protocol.

Western blot analysis

Cells or liver tissues were homogenized in lysis buffer (1% Nonidet P-40, 0.5% sodium deoxycholate, PBS, pH 7.4, 0.1% sodium dodecyl sulfate, 1× proteinase inhibitor cocktail (Nacalai Tesque) and 1× phosphatase inhibitor cocktail (Nacalai Tesque)). The supernatant was collected by centrifugation, and the protein concentration was measured using a bicinchoninic acid protein assay kit (Thermo Fisher Scientific). Equal amounts of the protein homogenates were separated in sodium dodecyl sulfate polyacrylamide gels and transferred onto a polyvinylidene fluoride membranes. Antibodies specific for the following proteins were used for immunodetection: COX IV (#4844), LDHA (#2012), cytochrome *c* (#11940), RIP1 (#3493), p-RIP1 (Ser166) (#31122), RIP3 (#14401), cleaved caspase-3 (#9661) and cleaved caspase-7 (#8438) purchased from Cell Signaling Technology; Mcl-1 (600-401-394) purchased from Rockland Immunochemicals (Limerick, PA, USA); β-actin (A5316) purchased from Sigma-Aldrich; MLKL (#MABC604) purchased from EMR Millipore; and p-MLKL (ab196436) purchased from Abcam. Protein expression was measured with ImageJ software.

Flow cytometric detection of apoptosis with annexin-V

To detect apoptotic cells, cells were suspended in annexin-V binding buffer (Biolegend, San Diego, CA, USA) and then stained with annexin-V and 7-AAD according to the manufacturer's protocol. Annexin-V-positive and 7-AAD-negative cells were defined as apoptotic cells.

Microarray analysis

Gene expression in L-Mcl-1-KO and L-Mcl-1/DNase II-KO mouse livers ($n = 3$ per group) was analyzed using a SurePrint G3 Mouse Gene Expression Kit (Agilent, Santa Clara, CA, USA). Genes that showed significant differential expression, defined as greater than a twofold difference,

were collected and further analyzed using pathway analysis (Ingenuity, QIAGEN, Hilden, Germany).

Primary hepatocyte isolation

Primary hepatocytes were isolated by the two-step pronase-collagenase perfusion of mouse livers as described previously [43]. Primary hepatocytes were maintained in William's Eagle medium (Gibco, Grand Island, NY, USA) containing 10% fetal calf serum, 2 mM L-glutamine (Gibco), 100 nM insulin (Sigma-Aldrich) and 100 nM dexamethasone (Sigma-Aldrich). Primary hepatocytes were isolated from *Bax*$^{flox/flox}$ *Bak*$^{-/-}$ *Alb-Cre* mice and from *Bax*$^{flox/flox}$ *Bak*$^{+/+}$ mice (wild-type mice). *Bax*$^{flox/flox}$ *Bak*$^{-/-}$ *Alb-Cre* mice have been described previously [44].

Statistical analysis

Data are shown as the mean ± standard deviation otherwise indicated. Statistical significance between two groups was assessed with an unpaired or paired two-sided Student's *t*-test. Multiple comparisons were performed by applying one-way analysis of variance (ANOVA) followed by Tukey's honest significant difference (HSD) test using JMP Pro 12 software (SAS Institute Inc., Cary, NC, USA). $P < 0.05$ was considered statistically significant.

Acknowledgements We sincerely thank AbbVie for providing ABT-737, Dr. S. Nagata (Kyoto University) for providing *Dnase2a* floxed mice, Dr. You-Wen He (Department of Immunology, Duke University Medical Center, Durham, NC) for providing the *Mcl-1* floxed mice and Dr. Kinya Otsu (King's College London) and Dr. Osamu Yamaguchi (Osaka University) for technical assistance with the measurement of DNase II activity using the SRED method.

Funding This work was partially supported by Grants-in-Aid for Scientific Research from the Ministry of Education, Culture, Sports, Science, and Technology of Japan (26253047 and 17H05508 to T Takehara and 17K09423 to HH) and a Grant-in-Aid for Research on Hepatitis from the Ministry of Health, Labour and Welfare of Japan.

Compliance with ethical standards

Conflict of interest The authors declare that they have no conflict of interest.

References

1. Malhi H, Guicciardi ME, Gores GJ. Hepatocyte death: a clear and present danger. Physiol Rev. 2010;90:1165–94.
2. Takehara T, Tatsumi T, Suzuki T, Rucker EB, Hennighausen L, Jinushi M, et al. Hepatocyte-specific disruption of Bcl-xL leads to continuous hepatocyte apoptosis and liver fibrotic responses. Gastroenterology. 2004;127:1189–97.
3. Vick B, Weber A, Urbanik T, Maass T, Teufel A, Krammer PH, et al. Knockout of myeloid cell leukemia-1 induces liver damage and increases apoptosis susceptibility of murine hepatocytes. Hepatology. 2009;49:627–36.
4. Kon K, Kim JS, Jaeschke H, Lemasters JJ. Mitochondrial permeability transition in acetaminophen-induced necrosis and apoptosis of cultured mouse hepatocytes. Hepatology. 2004;40:1170–9.
5. Masubuchi Y, Suda C, Horie T. Involvement of mitochondrial permeability transition in acetaminophen-induced liver injury in mice. J Hepatol. 2005;42:110–6.
6. Ramachandran A, McGill MR, Xie Y, Ni HM, Ding WX, Jaeschke H. Receptor interacting protein kinase 3 is a critical early mediator of acetaminophen-induced hepatocyte necrosis in mice. Hepatology. 2013;58:2099–108.
7. Galluzzi L, Vitale I, Abrams JM, Alnemri ES, Baehrecke EH, Blagosklonny MV, et al. Molecular definitions of cell death subroutines: recommendations of the Nomenclature Committee on Cell Death 2012. Cell Death Differ. 2012;19:107–20.
8. Tait SW, Green DR. Mitochondria and cell death: outer membrane permeabilization and beyond. Nat Rev Mol Cell Biol. 2010;11:621–32.
9. Rongvaux A, Jackson R, Harman CC, Li T, West AP, de Zoete MR, et al. Apoptotic caspases prevent the induction of type I interferons by mitochondrial DNA. Cell. 2014;159:1563–77.
10. White MJ, McArthur K, Metcalf D, Lane RM, Cambier JC, Herold MJ, et al. Apoptotic caspases suppress mtDNA-induced STING-mediated type I IFN production. Cell. 2014;159:1549–62.
11. Oka T, Hikoso S, Yamaguchi O, Taneike M, Takeda T, Tamai T, et al. Mitochondrial DNA that escapes from autophagy causes inflammation and heart failure. Nature. 2012;485:251–5.
12. Evans CJ, Aguilera RJ. DNase II: genes, enzymes and function. Gene. 2003;322:1–15.
13. Loomba R, Sanyal AJ. The global NAFLD epidemic. Nat Rev Gastroenterol Hepatol. 2013;10:686–90.
14. Feldstein AE, Canbay A, Angulo P, Taniai M, Burgart LJ, Lindor KD, et al. Hepatocyte apoptosis and fas expression are prominent features of human nonalcoholic steatohepatitis. Gastroenterology. 2003;125:437–43.
15. Malhi H, Gores GJ. Molecular mechanisms of lipotoxicity in nonalcoholic fatty liver disease. Semin Liver Dis. 2008;28:360–9.
16. Garcia-Monzon C, Martin-Perez E, Iacono OL, Fernandez-Bermejo M, Majano PL, Apolinario A, et al. Characterization of pathogenic and prognostic factors of nonalcoholic steatohepatitis associated with obesity. J Hepatol. 2000;33:716–24.
17. Dixon JB, Bhathal PS, O'Brien PE. Nonalcoholic fatty liver disease: predictors of nonalcoholic steatohepatitis and liver fibrosis in the severely obese. Gastroenterology. 2001;121:91–100.
18. Afonso MB, Rodrigues PM, Carvalho T, Caridade M, Borralho P, Cortez-Pinto H, et al. Necroptosis is a key pathogenic event in human and experimental murine models of non-alcoholic steatohepatitis. Clin Sci (Lond). 2015;129:721–39.
19. Gautheron J, Vucur M, Reisinger F, Cardenas DV, Roderburg C, Koppe C, et al. A positive feedback loop between RIP3 and JNK controls non-alcoholic steatohepatitis. EMBO Mol Med. 2014;6:1062–74.
20. Matzinger P. The danger model: a renewed sense of self. Science. 2002;296:301–5.
21. Chen GY, Nunez G. Sterile inflammation: sensing and reacting to damage. Nat Rev Immunol. 2010;10:826–37.
22. Luedde T, Kaplowitz N, Schwabe RF. Cell death and cell death responses in liver disease: mechanisms and clinical relevance. Gastroenterology. 2014;147:765–83.e764.
23. Gray MW, Burger G, Lang BF. Mitochondrial evolution. Science. 1999;283:1476–81.
24. Liu S, Gallo DJ, Green AM, Williams DL, Gong X, Shapiro RA, et al. Role of toll-like receptors in changes in gene expression and NF-kappa B activation in mouse hepatocytes stimulated with lipopolysaccharide. Infect Immun. 2002;70:3433–42.

25. Seki E, Brenner DA. Toll-like receptors and adaptor molecules in liver disease: update. Hepatology. 2008;48:322–35.
26. Uematsu S, Akira S. Toll-like receptors and Type I interferons. J Biol Chem. 2007;282:15319–23.
27. Hashiguchi K, Zhang-Akiyama QM. Establishment of human cell lines lacking mitochondrial DNA. Methods Mol Biol. 2009;554:383–91.
28. Hikita H, Takehara T, Shimizu S, Kodama T, Li W, Miyagi T, et al. Mcl-1 and Bcl-xL cooperatively maintain integrity of hepatocytes in developing and adult murine liver. Hepatology. 2009;50:1217–26.
29. Hikita H, Kodama T, Shimizu S, Li W, Shigekawa M, Tanaka S, et al. Bak deficiency inhibits liver carcinogenesis: a causal link between apoptosis and carcinogenesis. J Hepatol. 2012;57:92–100.
30. Tanaka S, Hikita H, Tatsumi T, Sakamori R, Nozaki Y, Sakane S, et al. Rubicon inhibits autophagy and accelerates hepatocyte apoptosis and lipid accumulation in nonalcoholic fatty liver disease in mice. Hepatology. 2016;64:1994–2014.
31. Kubes P, Mehal WZ. Sterile inflammation in the liver. Gastroenterology. 2012;143:1158–72.
32. Aizawa S, Contu VR, Fujiwara Y, Hase K, Kikuchi H, Kabuta C, et al. Lysosomal membrane protein SIDT2 mediates the direct uptake of DNA by lysosomes. Autophagy. 2017;13:218–22.
33. Barbalat R, Ewald SE, Mouchess ML, Barton GM. Nucleic acid recognition by the innate immune system. Annu Rev Immunol. 2011;29:185–214.
34. Cai X, Chiu YH, Chen ZJ. The cGAS-cGAMP-STING pathway of cytosolic DNA sensing and signaling. Mol Cell. 2014;54:289–96.
35. Garcia-Martinez I, Santoro N, Chen Y, Hoque R, Ouyang X, Caprio S, et al. Hepatocyte mitochondrial DNA drives nonalcoholic steatohepatitis by activation of TLR9. J Clin Invest. 2016;126:859–64.
36. Inami Y, Yamashina S, Izumi K, Ueno T, Tanida I, Ikejima K, et al. Hepatic steatosis inhibits autophagic proteolysis via impairment of autophagosomal acidification and cathepsin expression. Biochem Biophys Res Commun. 2011;412:618–25.
37. Ichim G, Lopez J, Ahmed SU, Muthalagu N, Giampazolias E, Delgado ME, et al. Limited mitochondrial permeabilization causes DNA damage and genomic instability in the absence of cell death. Mol Cell. 2015;57:860–72.
38. Kawane K, Ohtani M, Miwa K, Kizawa T, Kanbara Y, Yoshioka Y, et al. Chronic polyarthritis caused by mammalian DNA that escapes from degradation in macrophages. Nature. 2006;443:998–1002.
39. Yasuda T, Nadano D, Awazu S, Kishi K. Human urine deoxyribonuclease II (DNase II) isoenzymes: a novel immunoaffinity purification, biochemical multiplicity, genetic heterogeneity and broad distribution among tissues and body fluids. Biochim Biophys Acta. 1992;1119:185–93.
40. Koizumi T. Deoxyribonuclease II (DNase II) activity in mouse tissues and body fluids. Exp Anim. 1995;44:169–71.
41. Nakahira K, Haspel JA, Rathinam VA, Lee SJ, Dolinay T, Lam HC, et al. Autophagy proteins regulate innate immune responses by inhibiting the release of mitochondrial DNA mediated by the NALP3 inflammasome. Nat Immunol. 2011;12:222–30.
42. Ashley N, Harris D, Poulton J. Detection of mitochondrial DNA depletion in living human cells using PicoGreen staining. Exp Cell Res. 2005;303:432–46.
43. Kodama T, Takehara T, Hikita H, Shimizu S, Shigekawa M, Tsunematsu H, et al. Increases in p53 expression induce CTGF synthesis by mouse and human hepatocytes and result in liver fibrosis in mice. J Clin Invest. 2011;121:3343–56.
44. Hikita H, Takehara T, Kodama T, Shimizu S, Hosui A, Miyagi T, et al. BH3-only protein bid participates in the Bcl-2 network in healthy liver cells. Hepatology. 2009;50:1972–80.